Contents lists available at ScienceDirect

Journal of Alloys and Compounds

journal homepage: www.elsevier.com/locate/jallcom

Effect of Si content on surface hardening of Al–Si alloy by shot peening treatment

K.T. Cho[a], S. Yoo[b], K.M. Lim[c], H.S. Kim[d], W.B. Lee[a,*]

[a] Heat Treatment & Plating Technology Center, Korea Institute of Industrial Technology, Incheon 406-840, Republic of Korea
[b] Advanced Welding & Joining Technology Center, Korea Institute of Industrial Technology, Incheon 406-840, Republic of Korea
[c] Liquid Processing & Casting Technology R&D Department, Korea Institute of Industrial Technology, Incheon 406-840, Republic of Korea
[d] School of Materials Engineering, Inha University, 253, Younghyun-dong, Namgu, Incheon 402-751, Republic of Korea

ARTICLE INFO

ABSTRACT

The effect of Si content was investigated for Al–Si alloys (Al-7%, 11%, 18%Si) by shot peening process. The hardness increment by shot peening increased as the Si contents in Al–Si alloys increased. Finer Si particles and more dense distribution of those were observed in Al–18%Si than Al–7%Si. As Si contents of Al–Si alloys increased, grain size at the surface area of Al–Si alloy decreased. Higher hardness of Al–Si alloy with higher Si content could be attributable to more dense and refine Si particles and accelerated grain refinement during severe deformation.

© 2011 Elsevier B.V. All rights reserved.

1. Introduction

Aluminum–silicon alloy is widely used in automotive and aerospace industries due to its high strength with respect to weight, excellent castability, low density, etc. However, as compared with steel, Al–Si alloy has several problems such as low strength and wear properties, which limits the wide application of Al–Si alloy [1–3]. To overcome those disadvantages of Al–Si alloy, continuous attempts have been made over past decades. ECAP (Equal Channel Angular Pressing)/ECAE (Equal Channel Angular Extrusion) is one of the process techniques that enhance mechanical properties of Al alloys by severe plastic deformation [4–10]. MAO (micro-arc oxidation) [11], anodizing [12], PEO (Plasma Electrolytic Oxidation) [13], and plasma spray technique [14] are surface treatment techniques that employ plasma or electrochemistry to improve wear and corrosion properties of Al alloys. However, such processes for surface modification are only focused on chemical reaction.

Recently, there emerged an interesting physical surface treatment over past years, i.e. shot peening treatment that impacts metal particles to material surface to enhance surface properties [15–19]. Many researchers reported that shot peening refined surface grain, which enhanced the surface properties. Lu et al. introduced ultra-sonic shot peening (USSP) to improve surface properties of pure Fe [15] and 316L stainless steel [16]. They reported that severe deformation by USSP rearranged dislocations to form nano-sized sub-grains. They also found that USSP created nano-sized grains on the surface of 7075 Al alloy [17]. The grain refinement of 7075 Al alloy was due to the dislocation multiplication and rearrangement around Al_2Cu particles. Surface nanocrystallization was also studied by Umemoto's group [18,19]. It was revealed that surface nanocrystallization of carbon steels was formed by air blast shot peening. They suggested that larger strain amount and higher strain rate are favorable to form surface nanocrystallization.

Although a few studies were conducted on the shot peeing of Al alloys, most shot peening studies have focused on the surface nanocrystallization of steel and Al alloys. Besides, no shot peening research on widely-utilized Al–Si alloys has been reported for the surface hardening with varying Si contents. Therefore, the present study investigated the shot peening effect on the surface hardening of Al–Si alloy. To investigate the effect of Si contents, three different Al–Si alloys (A356, A336, A390) were used in this study. The mechanical properties and microstructural evolution of the Al–Si alloys were also investigated after shot peening process.

2. Experimental

The Al–Si alloys used in this study were A356, A336, and A390 and the chemical compositions of the Al–Si alloys are listed in Table 1. A cylindrically shaped specimen with the size of $\phi30 \times 10$ mm was cut and normalized to release residual stress that might be induced from casting and cutting process. Shot peening ball used in this study was rounded cut wire (RCW) ball with the diameter of 250 μm and the average hardness of shot balls was 760 HV. Shot balls were impacted perpendicu-

Table 1
Chemical composition of Al–Si alloy (wt%).

Al–Si alloys	Cu	Si	Mg	Zn	Mn	Fe	Ni	Ti	Al
A356 (Si 7%)	0.10	7.1	0.35	0.05	0.05	0.11	–	0.20	Balance
A336 (Si 11%)	1.07	11.4	0.997	0.813	0.005	0.175	2.004	0.004	Balance
A390 (Si 18%)	4.10	18.0	0.639	0.016	0.005	0.206	0.004	0.004	Balance

larly to the surface of Al–Si specimens at the pressure of 0.3 MPa. Microhardness of shot-peened specimens was measured by micro Vickers hardness tester (Future Tech FM-7). Microstructural evolution was observed by optical microscope (OM, Olympus BX51-33MU), scanning electron microscope (SEM, QUANTA 200F-EDAX) with energy dispersive X-ray spectrometer (EDS), and transmission electron microscope (TEM, JEOL2100). Specimens for TEM observation were prepared by focused ion beam (FIB, Helios Nanolab).

3. Results

Fig. 1 shows the surface hardness profile of three different Al–Si specimens as a function of shot peening time. The average surface hardness before shot peening was 65 HV for A356 and 80 HV for A336 and A390, respectively. The surface hardness was rapidly increased up to 60 s and then the slope of hardness increment gradually decreased up to 180 s. After 180 s, the hardness decreased slightly and saturated. From Fig. 1, it was noteworthy that the increment of surface hardness became higher as Si content of Al–Si alloy increased. The increment amounts of the surface hardness to maximum value were 90 HV, 110 HV, and 140 HV for A356, A336, and A390, respectively.

Cross-sectional optical micrographs before and after shot peening to Al–Si alloys are shown in Fig. 2. Before shot peening (Fig. 2a, e, i), matrix α and plate-shaped eutectic Si phase existed for all Al–Si specimens. The quantity of plate-shaped eutectic Si phase increased as Si content in Al–Si alloys increased. Coarse primary Si phase was observed only in A390 (designated as a white arrow in
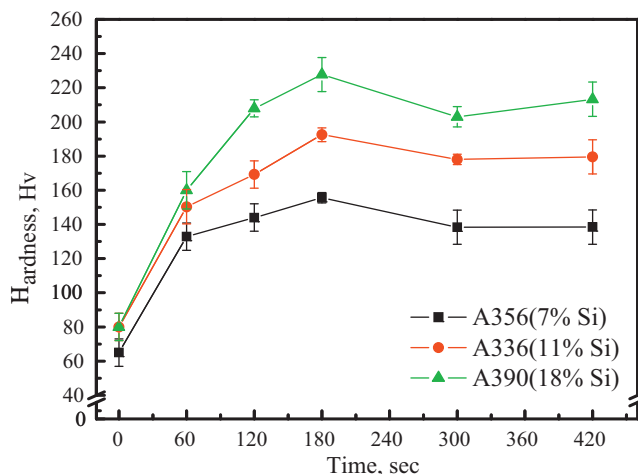

Fig. 1. Surface hardness profile with shot peening time.

Fig. 2) as well as plate-shaped eutectic Si phase. When Al–Si alloys were shot-peened, severe plastic deformation was observed in the near-surface region. As shot peening time increased, plate-shaped eutectic Si phase was refined in the surface region due to the intensive plastic strain energy. In addition, the primary Si phase of A390 was broken and spheroidized by severe plastic deformation.
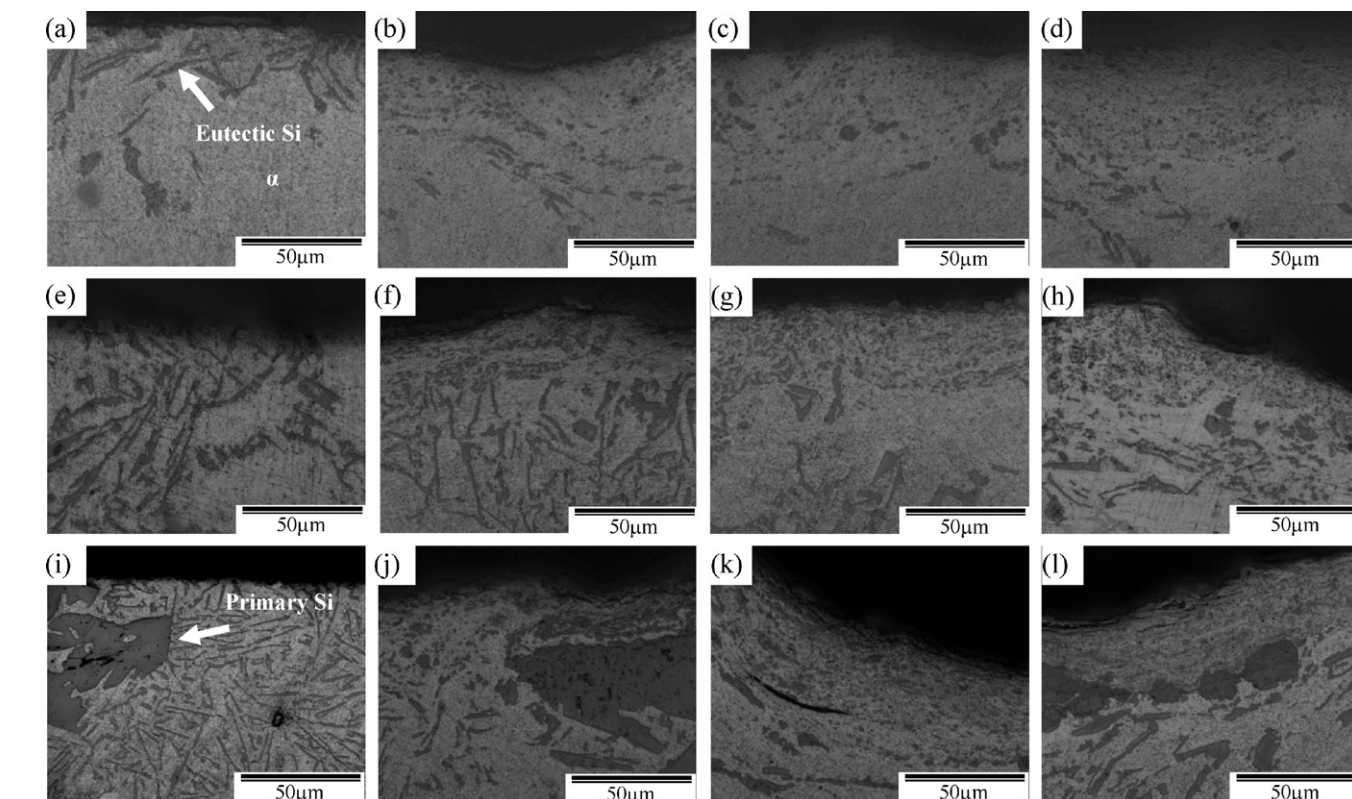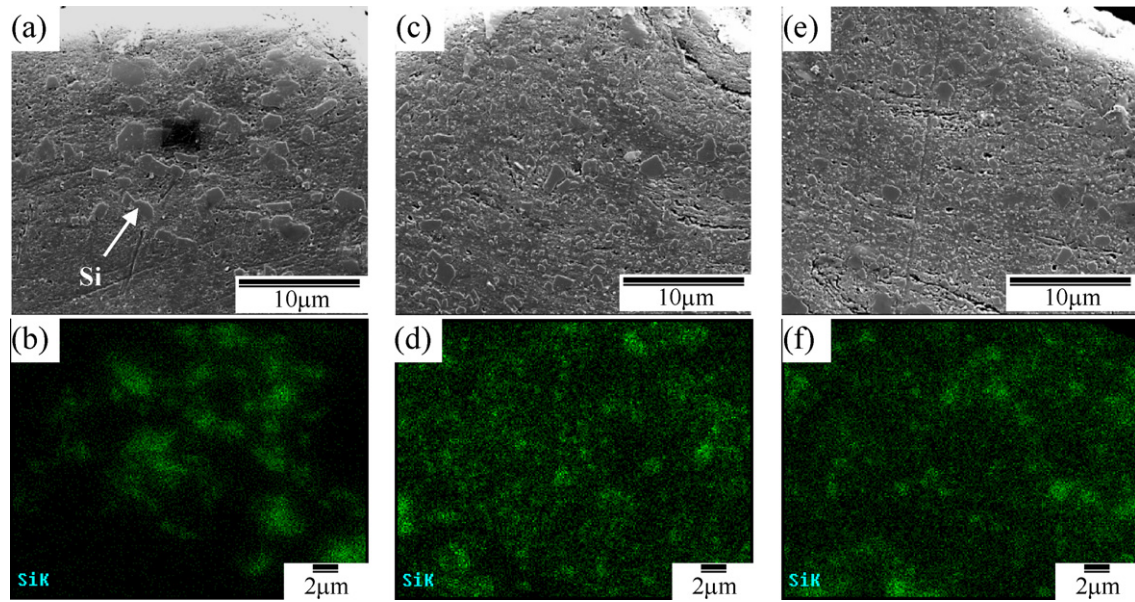

Fig. 2. Cross-sectional optical micrographs of A356 (7% Si, a–d), A336 (11% Si, e–h), and A390 (18% Si, i–l): as-cast (a, e, i) and shot peened for 60 s (b, f, j), 120 s (c, g, k), and 180 s (d, h, l).

Fig. 3. Cross sectional SEM micrograph and corresponding Si element area mapping images of shot peened A356 (7% Si, a and b), A336 (11% Si, c and d), and A390 (18% Si, e and f) for 180 s.
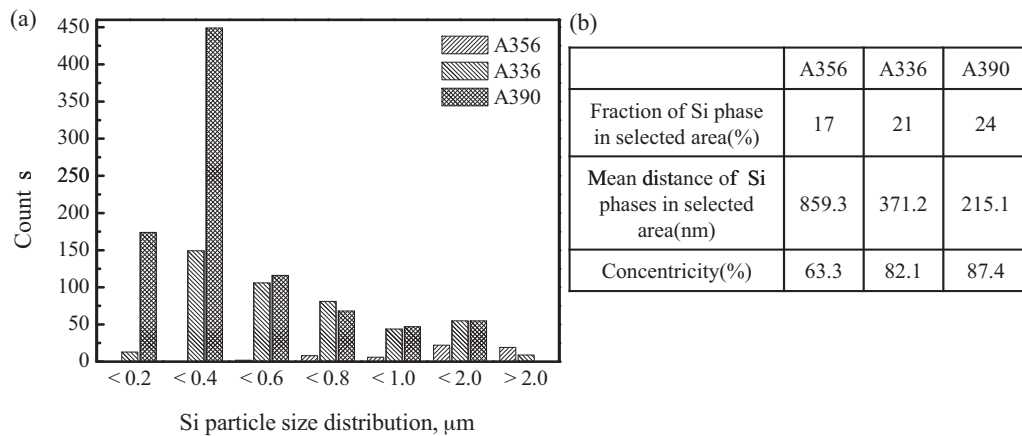

	A356	A336	A390
Fraction of Si phase in selected area(%)	17	21	24
Mean distance of Si phases in selected area(nm)	859.3	371.2	215.1
Concentricity(%)	63.3	82.1	87.4

Fig. 4. Si phase size distribution (a) and an analysis (b) showing fraction, mean inter-phase spacing, and concentricity of Si phase from the images of Fig. 3(a, c, e).

To observe refined Si particles by shot peening in detail, the shot-peened Al–Si specimens were observed with cross-sectional SEM and shown in Fig. 3. All specimens were shot-peened for 180 s. The refined Si particles were dispersed in the near-surface region. Fig. 4 shows particle size distribution of the Al–Si specimens after shot peening for 180 s. Nearly all Si particles of A356 (Si content: 7%) were larger than 1 μm. For A336 (Si contents: 11%) and A390 (Si content: 18%), most of the Si particles were <0.6 and 0.4 μm, respectively. Therefore, the size of the Si particles refined by the shot peening decreased as the Si content of Al–Si alloys increased.

Fig. 5 illustrates TEM micrographs of Al–Si specimens before and after shot peening. Coarse grains before shot peening treatment were observed from TEM. After shot peening, elongated grains were observed in the surface region. The formation of elongated grains was due to the severe plastic deformation of shot peening. Like refined Si particles, the grain size also decreased with the increase of Si content in Al–Si alloy. The average grain sizes of A356, A336 and A390 were about 263, 148, and 102 nm, respectively.

Fig. 6 shows TEM micrographs of shot-peened A390 alloy observed at various depths (0.5, 3.3, and 6.0 μm) from the surface.

The size of grains and Si particles increased as the observation point goes deeper from the surface. The size of eutectic-Si was about 50, 70 and 150 nm at the depth of 0.5, 3.3, and 6.0 μm from the surface, respectively. Furthermore, dense dislocations and refiner grains were observed around the refined Si particles.

4. Discussion

In this study, shot peening refined the surface grains and Si phase of the Al–Si alloys by severe plastic deformation. As shown in Figs. 2–4, Si particles were more refined by shot peening as Si content of Al–Si alloys increased. Such refinement of Si particles in Al alloys was also shown in Rotary Die-Equal Channel Angular Pressing (RD-ECAP) research [20,21]. In the RD-ECAP process, more refined Si particles were observed in Al–23%Si alloy than in Al–11%Si alloy.

The refined Si particle formed by severe plastic deformation played a role as a site of dislocation multiplication. Morris et al. [4,6] also reported mechanical properties increased as Si content of Al alloys increased during ECAP process. They suggested that the grain refinement was due to the multiplication
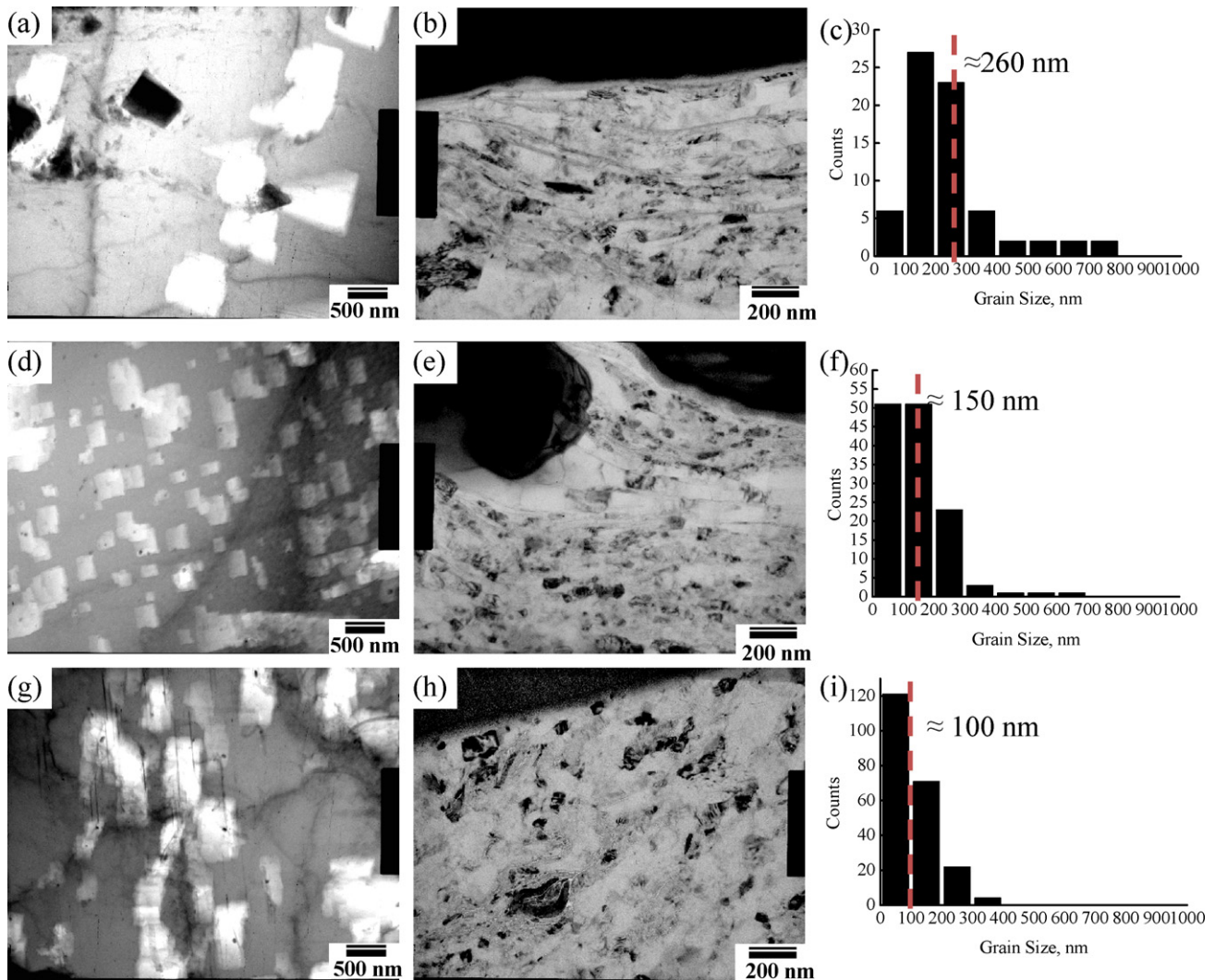
Fig. 5. TEM images and grain size analysis of A356 (7% Si, a–c), A336 (11% Si, d–f), and A390 (18% Si, g–i) before (a, d, g) and after shot peening for 180 s (b, e, h).

and rearrangement of dislocations around Si particles. In the present study, dense dislocations (Fig. 6(c)) around Si particles indicated that the Si particles served as sites of dislocation multiplication during severe plastic deformation of shot peening.

Fig. 7 shows schematic drawings of the grain refinement process for hypo- and hyper-eutectic Al–Si alloys during shot peening. When shot peening process is applied onto Al–Si alloy, eutectic-Si particles were refined and dispersed in the matrix. As shot peening time increased, the size of Si particles gradually decreased and dispersed in surface region. In case of hyper-eutectic alloy, primary Si phase was also broken to produce refined particles. At the same time, dislocations also were generated at the interface of Al/Si phase by the severe defor-
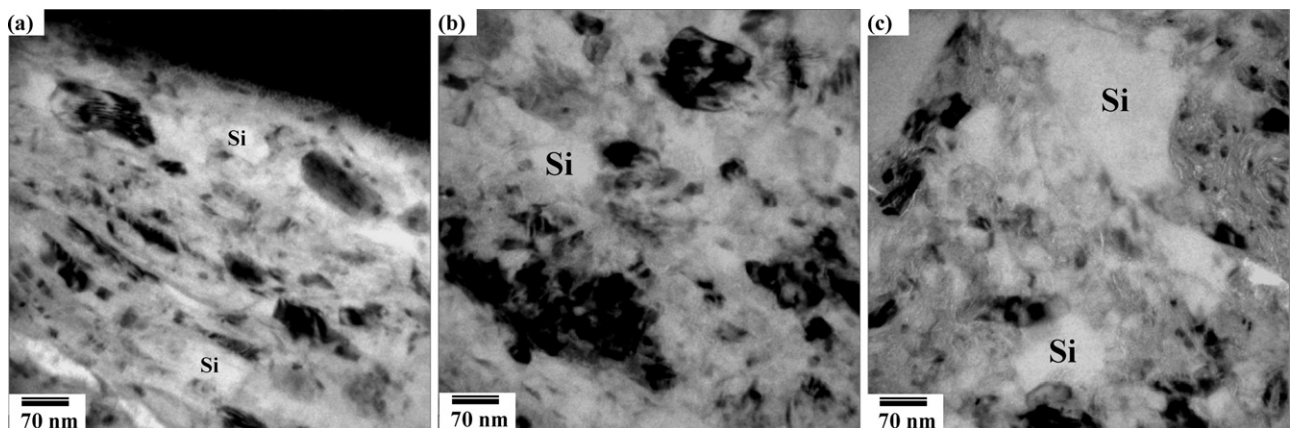

Fig. 6. TEM images of shot peened A390 covering various distances from the surface: (a) at 0.5 μm, (b) at 3.3 μm, and (c) at the 6.0 μm from the surface.
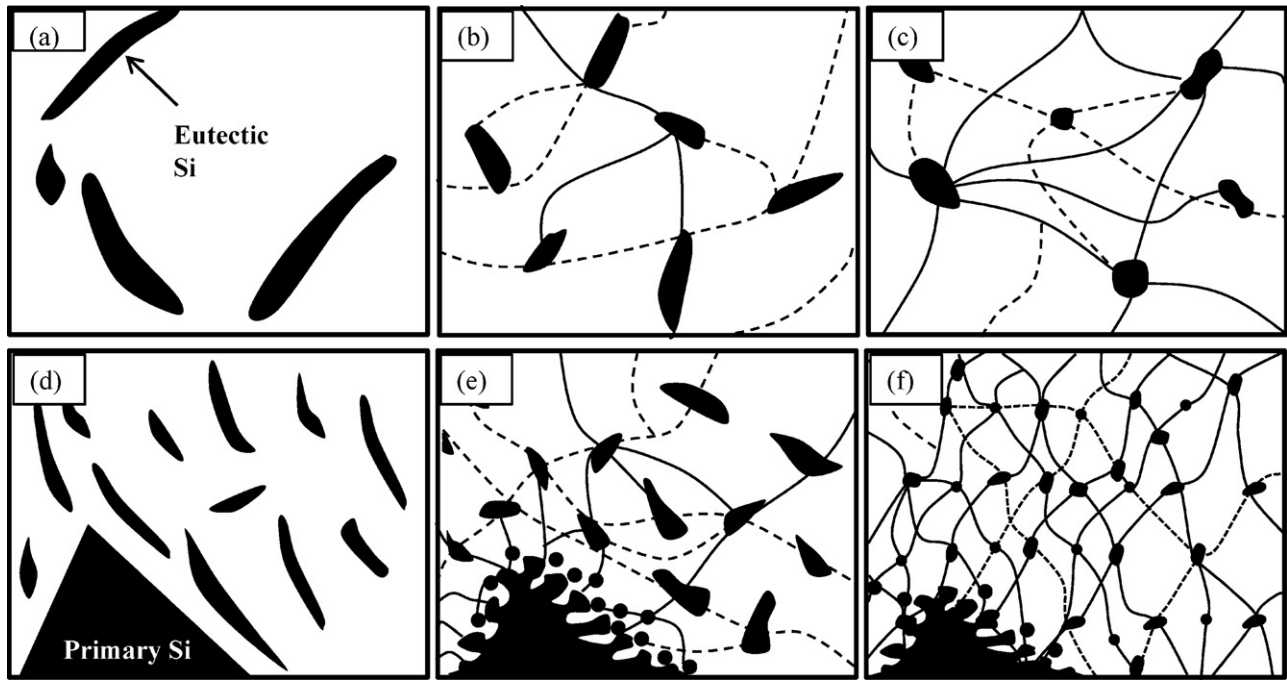
Fig. 7. Schematics showing grain refinement and hardening mechanisms of Al–Si alloy along with increase of shot peening time: (a–c) hypo-eutectic Al–Si alloy, (d–f) hyper-eutectic Al–Si alloy (⬤, silicon particle; —, grain boundary; - - -, sub-grain boundary).

mation during shot peening. The generated dislocations were rearranged by further energy from shot peening process and the rearrangement finally formed sub-grain boundaries and grain boundaries, as in the case of the literature [4,6,15,17]. Therefore, the newly-formed grain boundaries led to the grain refinement during shot peening process. Since the refined Si particles of the hyper-eutectic Al–Si alloy (high Si content alloy) were more densely dispersed than that of hypo-eutectic Al–Si alloy (low Si content alloy), the more dislocations were generated during shot peening. Hence, more grain boundaries were generated in the hyper-eutectic alloy than in the hypo-eutectic alloy, which resulted in more refined grains in the hyper-eutectic alloy.

The refined Si particles served as dislocation barriers by pinning the moving dislocations. The interparticle distance, λ, was calculated by the following equation:

$$\lambda = \frac{4(1-f)r}{3f}$$

where f and r are the volume fraction and radius of particles, respectively. The calculated interparticle distances of refined Si particles were 859, 375, and 215 nm for A356, A336 and A390, respectively (Fig. 4(b)). In other words, interparticle distance decreased as Si content of Al–Si increased, and it resulted in strong dispersion hardening effect for the high Si content alloy. Hence, this could contribute to achieving higher hardness of Al–Si alloy with higher Si content. Besides, the grain refinement was dominant for the high Si content alloy (hyper-eutectic Al–Si) as explained in Fig. 7. Therefore, the high increment of surface hardening for high Si content alloy was due to the densely dispersed Si particles and the refined grains from dislocation rearrangement around the Si particles during shot peening.

5. Conclusion

This study investigated the effect of Si contents on the surface hardening of Al–Si alloy by shot peening process. The increment of surface hardness of Al–Si alloys increased as Si contents increased. Broken and dispersed Si particles from eutectic and primary Si phase are formed by severe plastic deformation. As Si content of Al–Si alloys increased, more refined and densely dispersed Si particles were observed at the surface area. Dense dislocations were generated around the refined Si particles, which indicated that Si particles served as dislocation generation sites. The grain refinement was accelerated due to the rearrangement of dislocation around dispersed Si particles. The high increment of surface hardness as Si content increased was due to the increased Si particles and grain refinement accelerated by the increased Si particles.

Acknowledgement

References

[1] Q.G. Wang, Met. Mater. Trans. 34A (2003) 2887.
[2] T. Wei, F. Yan, J. Tian, J. Alloys Compd. 389 (2005) 169–175.
[3] X. Sum, Z. Jiang, S. Xin, Z. Yao, Thin Fold Film 471 (2005) 194–199.
[4] I. Gutierrez-Urrutia, M.A. Munoz-Morris, D.G. Morris, Acta Mater. 55 (2007) 1319–1330.
[5] D.G. Morris, M.A. Munoz-Morris, Acta Mater. 50 (2002) 4047–4060.
[6] M.A. Munoz Morris, I. Gutierrez-Urrutia, D.G. Morris, Mater. Sci. Eng. A 493 (2008) 141–147.
[7] P.J. Apps, J.R. Bowen, P.B. Prangnell, Acta Mater. 51 (2003) 2811–2822.
[8] I. Gutierrez-Urrutia, M.A. Munox-Morris, D.G. Morris, Mater. Sci. Eng. A 394 (2005) 399–410.
[9] B.B. Straumal, B. Baretzky, A.A. Mazilkin, F. Phillipp, O.A. Kogtenkova, M.N. Volkov, R.Z. Valiev, Acta Mater. 52 (2004) 4469–4478.
[10] C. Xu, M. Furukawa, Z. Horita, T.G. Landon, Acta Mater. 51 (2003) 6139–6149.
[11] M.H. Zhu, Z.B. Cai, X.Z. Lin, P.D. Ren, J. Tan, Z.R. Zhou, Wear 263 (2007) 472–480.

[12] J. Koneczy, L.A. Dobrazanski, K. Labisz, J. Duszczyk, J. Mater. Process. Technol. 157–158 (2004) 718–723.

[13] J. He, Q.Z. Cai, H.H. Luo, L. Yu, B.K. Wei, J. Alloys Compd. 471 (2009) 395–399.

[14] O. Sarikaya, S. Anik, S. Aslanlar, S. Cem Okumus, E. Celik, Mater. Des. 28 (2007) 2443–3449.

[15] N.R. Tao, M.L. Sui, J. Lu, K. Lu, NanoStruct. Mater. 11 (1999), 443–440.

[16] G. Liu, J. Lu, K. Lu, Mater. Sci. Eng. A 286 (2000) 91–95.

[17] X. Wu, N. Tao, Y. Hong, B. Xu, J. Lu, K. Lu, Acta Mater. 50 (2002) 2075–2084.

[18] M. Umemoto, Mater. Trans. 44 (2003) 1900–1911.

[19] J.L. Liu, M. Umemoto, Y. Todaka, K. Tsuchiya, J. Mater. Sci. 42 (2007) 7716–7720.

[20] A. Ma, K. Suzuki, Y. Nishida, N. Saito, I. Shigematsu, M. Takagi, H. Iwata, A. Watazu, T. Imura, Acta Mater. 53 (2005) 211–220.

[21] A. Ma, K. Suzuki, N. Saito, Y. Nishida, M. Takagi, I. Shigematsu, H. Iwata, Mater. Sci. Eng. A 399 (2005) 181–189.